ACS OMEGA

http://pubs.acs.org/journal/acsodf

Article

Experimental Investigation of CO_2-Induced Silica Gel as the Water Blocking Grout Effect of Aquifer Ions

Ichhuy Ngo,* Liqiang Ma,* Jiangtao Zhai, Yangyang Wang, Tianxiang Wei, and Yanxiao Ni

Cite This: *ACS Omega* 2022, 7, 27090−27101

Read Online

ACCESS | Metrics & More | Article Recommendations

ABSTRACT: This study aimed to prevent water flow in microcracks and simultaneously achieve CO_2 capture during grouting (CCG). Using sodium silicate (SS) as the primary material, the microcracks were grouted by a two-step approach. The low-initial-viscosity (5 mPa s) SS was first saturated within the microcracks followed by CO_2 injection at 2 MPa. Through CO_2 dissolution, silica gel was developed and tolerated a hydraulic pressure of up to 5.5 MPa. The effects of aquifer ions (Na^+, Ca^{2+}, Mg^{2+}, HCO_3^-, and SO_4^{2-}) were equally evaluated at harsh conditions, and it was found that the strength of the silica gel was reduced, which was caused by salting out, low CO_2 solubility, and precipitation. As a result, the hydraulic pressure was reduced to as low as 3 MPa. After 210 days, 16% of the silica gels (without ion inclusion) were reversible to the liquid phase, where a similar effect was found in the cases of Na^+ and Mg^{2+} ions. The degradation increased with more Ca^{2+} ions (up to 55%) and decreased with more HCO_3^- and SO_4^{2-} ions. Microcracks grouted with CCG extended the CO_2 utilization in grouting application. Combined with the effect of dissolved ions, the proposed approach is feasible in the field implementation for underground engineering under water bodies.

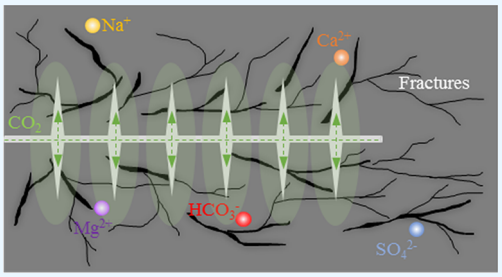

1. INTRODUCTION

China's energy consumption mainly relies on coal production.[1] As "green development" becomes a social norm and national strategy, ecological considerations in coal mining have become a hot topic of concern.[2] From 2013, additional attention has been paid to the ecology of the coal mine with the implementation of "The Belt and Road Initiative".[3] Water protection is among the most important measures to conduct coal mining in arid and semiarid areas. In underground coal mining, after the coal seam has been mined, the roof and floor rock of the mine area lose their equilibrium, resulting in deformation, destruction, and fracture of the surrounding rock strata.[4] This leads to water resource losses if left untreated. Many researchers[5−7] addressed this issue by three main approaches, namely, water conservation mining, underground reservoir storage, and simultaneous exploitation of coal and groundwater.[8] However, these methods could not perfectly prevent the flow of water down the mine goaf, unless they are cotreated with a grouting material.[9−11]

Currently, the available grouting materials could not effectively grout the more complex hydrogeological conditions for groundwater control.[12] Traditional cement grouting with standard methods could not seal the fissures to an acceptable level in certain advanced grouting requirements. Microcracks are also a flowing path that needs to be treated during coal mining in water bodies.[13−15] The minimum fissure aperture that traditional suspensions (such as cement slurry and ultrafine cement slurry) can penetrate is approximately 50 to 100 μm, and the permeability coefficient of injection parts is 10^{-1} to 10^{-2} cm/s. The microfissures and low permeability strata cannot be effectively grouted, which leads to poor sealing of rock fissures and large residual water inflow after grouting.[16−18] Many researchers[19−21] found that microfractures are preferential pathways for fluid flow. Furthermore, the fracture is subjected to expansion through a leaching process by the water−rock interaction.[22,23] Hence, microcracks should be sealed to achieve water protection.

Sodium silicate (SS) is a common grouting material that is catalyzed by various agents. Zullo et al.[24] achieved low-pressure grouting in historical sites using SS activated by $NaHCO_3$. Li et al.[25] later investigated a mixture of polyurethane and SS to reinforce subsea tunnels. Seawater was found to reduce the peak strength of the grout by 10.9%. Furthermore, SS was also implemented in the drilling application. Coupled with glycerol triacetate or 1,4-butyrolactone, SS was feasible to achieve grouting while drilling (GWD) in a loose coal bed for the application of methane drainage.[26] In the oil and gas industry, SS is widely implemented as the plugging agent in naturally fractured formation.[27,28] Liu and Ott[29] reviewed the use of SS to isolate CO_2-rich formation. An amorphous silica gel was

Received: January 2, 2022
Accepted: July 4, 2022
Published: July 30, 2022

developed by lowering the pH of SS with CO_2 dissolution, through the reaction between SS and CO_2 (eq 1).

$$Na_2SOi_3 + CO_2 \rightarrow SiO_{2(gel)} + Na_2CO_3 \quad (1)$$

Regarding the efforts mentioned above by various researchers, SS is a potential material for CO_2 capture, and the developed silica gel can then be used to decrease the hydraulic conductivity. However, its stability with respect to dissolved ions within the formation of groundwater has not been well-investigated. The degradation of the developed silica gel also remained unclear when the ions are involved. Therefore, this study aims at investigating the grouting efficiency of silica gel developed by the reaction between CO_2 and SS. The study began with the rheological measurements of the silica gel considering the effect of ions. Then, grouting was conducted by a novel two-step approach. The degradation of silica gel was equally evaluated to ensure its application for the reduction of the hydraulic conductivity of coal mining under water bodies. The success of this study enables a novel means to achieve CO_2 capture while grouting (CCG), therefore standing as a potential criterion to achieve carbon neutrality in the China schedule in 2060.[30]

2. MATERIALS AND METHODS

2.1. Materials. Aquifer water (AW) was acquired from a coal mine located in Gaoping City, Shanxi Province, China. The aquifer water was analyzed for its constituents using inductively coupled plasma-mass spectrometry (ICP-MS, model 7900, Agilent Technology, United States). The dissolved ions are given in Table 1. Ionic water was then synthesized in-house from

Table 1. Composition of Aquifer Water (in ppm)

Na^+	Ca^{2+}	Mg^{2+}	Cl^-	HCO_3^-	SO_4^{2-}	pH
347.77	130.45	5.06	57.79	967.40	126.42	8.2

sodium chloride (NaCl), calcium chloride ($CaCl_2$), magnesium chloride ($MgCl_2$), sodium hydrogen carbonate ($NaHCO_3$), and sodium sulfate (Na_2SO_4), all supplied by Sigma-Aldrich.

Sodium silicate (SS) was purchased from Tianjin Hengxing Chemical Reagents Co., Ltd., 99.99% pure. The fundamental properties of SS are given in Table 2.

Table 2. Fundamental Properties of SS

characteristics	value
total Na_2O, % by mass	19.3
Na_2O in silicate, % by mass	22.8
total SiO_2, % by mass	23.5
Na_2O/SiO_2 ratio	1.03
viscosity, mPa s (in 1% solution, 20 °C)	4.5
acidity, pH unit (in 1% solution)	8.3
density, g/cm^3	2.4

Fractured rock was tested for its oxide composition that was determined by X-ray fluorescence spectroscopy (XRF, model S8 Tiger spectrometer, Bruker, Germany) as given in Table 3.

Table 3. Oxide Composition of the Rock Sample

SiO_2	Al_2O_3	Na_2O	Fe_2O_3	K_2O	MgO	CaO	other
68.85	17.17	4.55	2.41	3.16	0.73	1.51	1.62

2.2. Preparation. The SS solution was formulated by dissolving 10 g of SS in 100 mL of deionized water (DW). Ten aliquots of the SS solution were diluted from the base solution in a range from 1 to 10% by weight.

The effects of ions were investigated with respect to the compositions of aquifer water. For instance, Na^+ ranged from 200 to 1000 ppm, Ca^{2+} ranged from 50 to 1000 ppm, Mg^{2+} ranged from 50 to 1000 ppm, HCO_3^- ranged from 200 to 2000 ppm, and SO_4^{2-} ranged from 50 to 1000 ppm. The defined concentration of ions was dissolved in DW before adding SS.

The core sample was first cleaned in a 40 kHz sonication bath for 30 min and then dried in an oven at a constant temperature of 105 °C for 8 h to remove the residue water, after which the porosity (voids and fractures) of the sample was determined by the fluid saturation method.

2.3. Methods. A series of laboratory experiments were carried out to investigate the reduction behaviors in the hydraulic conductivity of CO_2-induced silica gel in the fractured sample considering the effect of dissolved ions on the water of the aquifer. The experiment procedure is demonstrated in Figure 1.

2.3.1. Dynamic Rheological Test. Dynamic rheological properties were measured using the apparatus shown in Figure 2. Prior to testing, 30 mL of a defined concentration of SS solution was transferred to the reaction tank. After that, CO_2 gas was bubbled within the tank at a constant rate of 1 L/min, while the dynamic viscosity and pH of the mixture were monitored using an NDJ-1 viscometer (shear rate of 100 s^{-1}) and a pH meter connected at the outflow of the reaction tank. Data were recorded every minute. Once the silica gel formed, as visually observed, the shear rate was reduced to 50, 20, and 10 s^{-1} to investigate the fluid behavior.

The effects of water ions from the aquifer were investigated on the viscosity of the silica gel. This included the required reaction time (gel time), pH changes, and concentration of the ions.

2.3.2. Grouting Test. The core sample was mounted in a Hassler core holder as shown in Figure 3.

Prior to the grouting experiment, the initial permeability of the core was determined. Deionized water was injected at constant rates of 0.5, 1, and 1.5 mL/min to flow through the fractured samples. The absolute permeability was then calculated following Darcy's law:

$$Q = \frac{K_{abs}}{\mu} \times \frac{A\Delta P}{L} \quad (2)$$

where Q is the flow rate (m^3/s), K_{abs} is the absolute permeability (m^2), μ is the water viscosity (N s/m^2), A is the cross section of the core (m^2), ΔP is the pressure change across the column (MPa), and L is the length of the core (m).

A total of seven grout tests were performed to evaluate the efficiency of silica gel as a hydraulic conductivity reduction agent formulated from a reaction between CO_2 and the SS solution. Dissolved anions and cations were equally considered in this work. In the base case, DW was first imbibed into the sample at a flow rate of 0.5 mL/min until saturated, observed without air bubbles forming in the fluid collector. After that, the injection was shifted to the SS solution while the injection rate remained unchanged. To ensure that the in situ SS reached the designed concentration, the SS concentration in the fluid collector was monitored. Then, the production valve was shut in while the injection was shifted to CO_2 gas. The injection was carried out until the column pressure reached 2 MPa. The CO_2 gas and the

https://doi.org/10.1021/acsomega.2c00019
ACS Omega 2022, 7, 27090−27101

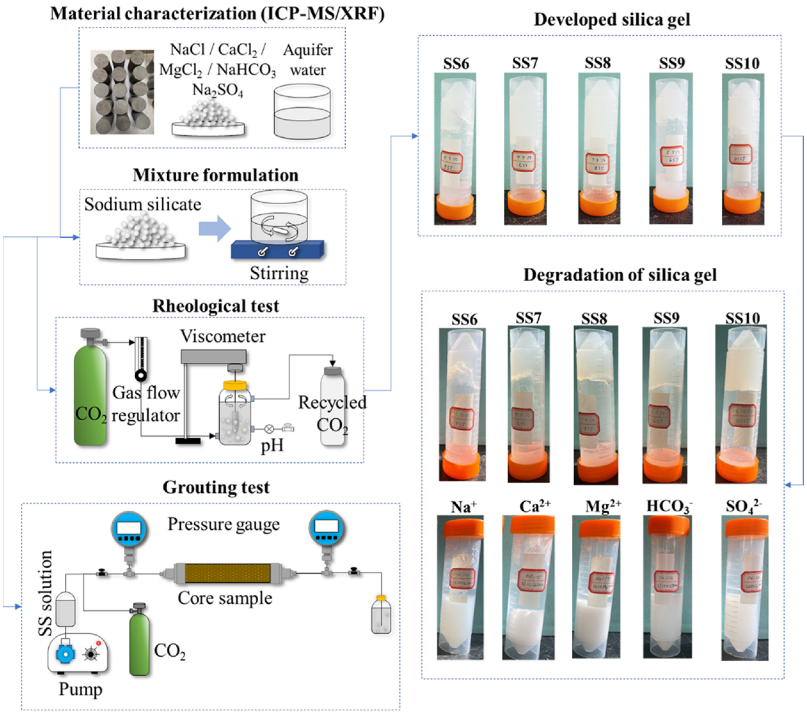

Figure 1. Experimental flow chart.

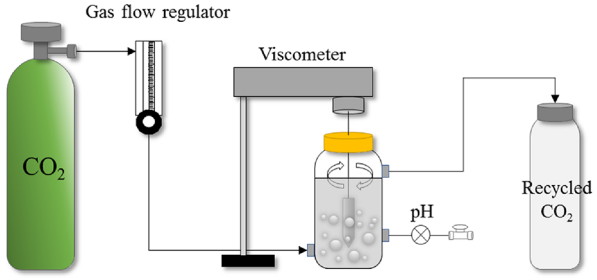

Figure 2. Dynamic rheological properties and pH monitoring during the reaction.

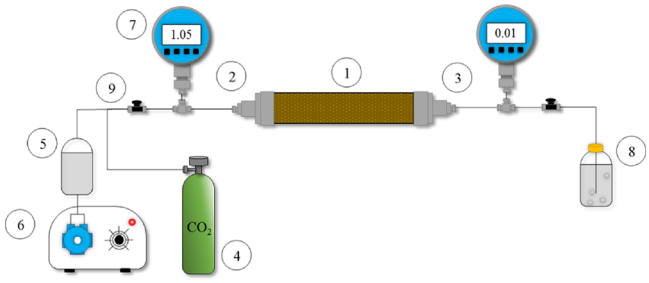

Figure 3. Schematic representation of the water blocking apparatus; (1) a Hassler core holder, (2) an injecting end, (3) a producing end, (4) a CO_2 gas tank, (5) a jacketed cell containing injected fluids, (6) a pump, (7) a pressure gauge, (8) a fluid collector, and (9) a valve.

in situ SS in the system were allowed to react until equilibrium, observed by a pressure change below 5%.

The effects of dissolved ions and AW on the current approach were evaluated using ionic water (Na^+, Ca^{2+}, Mg^{2+}, HCO_3^-, and SO_4^{2-}) at their maximum concentration in this study and the synthesized AW, where the injection sequence is given in Figure 4. The core was first saturated with various ionic water or AW (0 to 10 min). After which, the SS solution was injected. The

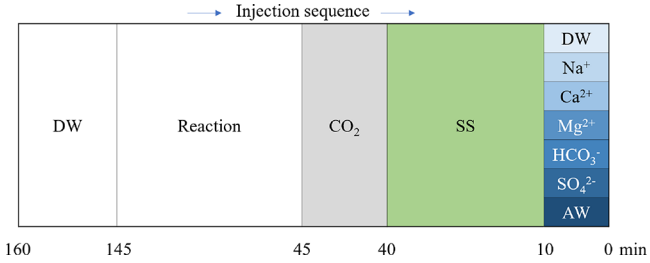

Figure 4. Illustration of the injection scenarios.

producing end was shut in at 40 min while CO_2 gas was fed into the column. It took approximately 5 min to reach 2 MPa. Then, the column was left for the reaction, and the pressure of the column was monitored. After equilibrium, the producing end was opened, and deionized water was injected to determine the permeability of the core after grouting and the maximum injecting pressure that the grouted column could tolerate.

2.3.3. Permeability Test. The permeability test was conducted in a sense to measure the hydraulic conductivity of the core sample after the grouting test. Upon equilibrium pressure, DW was injected into the core sample to determine permeability after grouting. The water injection rate was increased stepwise to measure the maximum injection pressure that the grouted core sample could tolerate. Furthermore, the change in the sample permeability was calculated following Darcy's law given in eq 2.

2.3.4. CO_2 Solubility Test. Prior to the grouting test, the total porosity of the sample was determined. Thus, the mole of CO_2 injected into the sample, n_{CO_2}, was calculated by the Peng–Robinson cubic equation of state. The equilibrium pressure, P_e, was measured when there was no observed pressure change. The partial pressure of CO_2 in the vapor phase was determined by assuming that the phase obeyed Dalton's law and was therefore

https://doi.org/10.1021/acsomega.2c00019
ACS Omega 2022, 7, 27090−27101

expressed as the difference between the total equilibrium pressure and the pressure of the aqueous solution free of CO_2.

$$P_{CO_2} = P_i - P_e \quad (3)$$

where P_i is the initial pressure.

The amount of CO_2, $n_{CO_2(g)}$, remaining in the gas phase was calculated using the Peng−Robinson cubic equation of state with the known P_{CO_2}, temperature, and volume of the gas phase. The amount of dissolved CO_2 in the liquid phase was calculated as follows:

$$n_{CO_2(l)} = n_{CO_2} - n_{CO_2(g)} \quad (4)$$

The solubility of CO_2 within SS solution was thereby calculated using eq 5 as follows:

$$S_{CO_2} = \frac{n_{CO_2(l)}}{V_{void}} \quad (5)$$

where S_{CO_2} is the solubility of CO_2 within the solution (mol/cm^3) and V_{void} is the volume of the porosity and fracture of the rock sample (cm^3).

2.3.5. Degradation of Silica Gel. The degradation of silica gel was investigated by measuring the concentration of silica in its initial stage and upon stepwise reduction after 7, 30, 90, and 210 days in gelled samples using ICP-MS.

3. RESULTS AND DISCUSSION

3.1. Rheological Properties. Silica gel was formulated by the dissolution of CO_2 in sodium silicate solution. The rheological properties of the reacted mixture were measured. The results are shown in Figure 5.

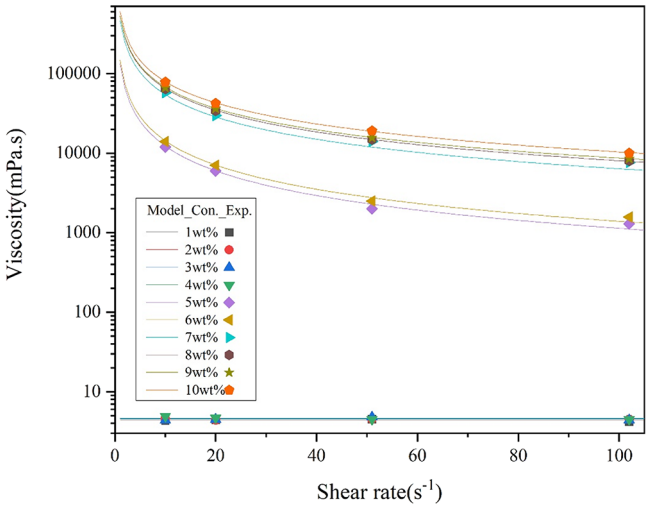

Figure 5. Steady shear flow of silica gel with different concentrations of SS.

It is observed that after the CO_2 reaction, the viscosity of the SS solution at the concentration from 1 to 4 wt % remained unchanged by increasing the shear rate from 10 to 100 s^{-1}, which could thus be described as the Newtonian fluid.[31] At a higher concentration of SS from 5 to 10 wt %, the experimental measurements were found to better agree with the power law model, where the minimum R^2 was 0.998 (Table 4). Therefore, the power law could be utilized to represent the silica gel and is expressed as follows.

$$\mu_a = K(\gamma)^{n-1} \quad (6)$$

where μ_a is the apparent viscosity, K is the consistency index, γ is the shear rate, and n is a flow behavior index. When $n < 1$, the mixture has the characteristic of shear thinning and can be defined further as a pseudoplastic fluid, when $n = 1$, the mixture has the characteristic of a Newtonian fluid, and when $n > 1$, the mixture has the characteristic of shear thickening and can be described as a dilatant fluid.

As shown in Table 4, the consistency index K value of the silica gel increased from 4.35 to 4.65 mPa s^n by increasing the SS concentration from 1 to 4 wt %, respectively. The K value was significantly lower than that of other cases where the concentration was beyond 5 wt %. This was due to the fact that in this SS concentration range, no silica gel was formed, as shown in Figure 6. Basically, the aqueous form of sodium silicate possesses dissolved silica (SiO_2), dissolved alkali (Na_2O), and water (H_2O). Once the silica molecule contacts with the acid, neutralization of stabilizing alkali occurs and silicate anions form polymeric silica connected by the Si−O−Si bond with expulsion of water molecules (Figure 7a). This action creates a silica sol (or colloidal silicate particles), and consequently, these sol particles aggregate to form gels[32] (Figure 7b). In the same sense, as CO_2 dissolves in water, the developed carbonic acid (H_2CO_3) reduces the pH of the system, and polymerization then occurs. At a concentration over 5 wt %, the K value was 133,224.11 mPa s^n and increased to 607,078.86 mPa s^n at 10 wt %. Undoubtedly, this indicates the formation of a silica gel. This implies that the concentrated sodium silicate in the suspension increases its overall density. So, more sol is developed after the CO_2 reaction and later agglomerated into gels.

The flow behavior index, n, of the silica gel could be classified into three groups. In the ungelled group (1 to 4 wt %), viscosity was not affected by increasing the shear rate. The gelled group at a concentration between 5 and 6 wt % possessed the shear thinning characteristic, but the value was negative. This was plausibly due to the molecular degradation of the sample, which is well-reported in the literature.[33,34] The gelled group at a concentration of 7 to 10 wt % also had shear thinning characteristics, where the n value increased by including a higher SS content, indicating a greater gel strength. In this regard, a higher concentration of SS is more suitable to be applied as a grouting gel to reduce hydraulic conductivity in microcracks.

Further investigation of the effect of SS concentration on gel time is shown in Figure 8. The gel time was observed to be 15 min for concentrations between 5 and 7 wt %. It was reduced to 13 min by increasing the concentration to 8 and 9 wt %. However, at the highest concentration in this study, the gel time increased again to 15 min. There was a greater resistance of the CO_2 gas to dissolve within the solution at a higher concentration closer to its saturation point. The same mechanism was explained by the use of salted water.[35]

As shown in Figure 9a, the dissolution of CO_2 within the mixture is a continuous process that results in a gradual decrease in pH. It was observed that the viscosity of the SS solution remained unchanged in the concentration range from 1 to 4 wt %, while there was a rapid increase in viscosity at a certain pH in the concentration range from 5 to 10 wt %. At a lower concentration of SS, the dissolved silicate is not able to agglomerate during the neutralization, so the silica gel did not form. In other words, higher-concentration cases possessed more silicate, which facilitates the agglomeration of the silica gel.

https://doi.org/10.1021/acsomega.2c00019
ACS Omega 2022, 7, 27090−27101

Table 4. Rheological Parameters of the Reacted SS Solution

			K (mPa s^n)		n		R^2
conc. (wt %)	model	fitting result	model	exp.	model	exp.	
1	Newtonian	$\tau = 4.35\gamma$	4.35	4.28	1	1	1
2		$\tau = 4.50\gamma$	4.50	4.51	1	1	1
3		$\tau = 4.53\gamma$	4.53	4.54	1	1	1
4		$\tau = 4.65\gamma$	4.65	4.67	1	1	1
5	power law	$\tau = 133{,}224.11\gamma^{-1.035}$	133,224.11	134,035.75	−0.035	−0.032	0.998
6		$\tau = 146{,}928.92\gamma^{-1.012}$	146,928.92	145,529.12	−0.012	−0.013	0.998
7	pseudoplastic	$\tau = 465{,}179.10\gamma^{-0.932}$	465,179.10	466,854.63	0.068	0.070	0.999
8		$\tau = 528{,}128.26\gamma^{-0.909}$	528,128.26	527,714.52	0.091	0.088	0.999
9		$\tau = 530{,}818.33\gamma^{-0.894}$	530,818.33	531,768.39	0.106	0.107	0.999
10		$\tau = 607{,}078.86\gamma^{-0.884}$	607,078.86	606,948.46	0.116	0.115	0.999

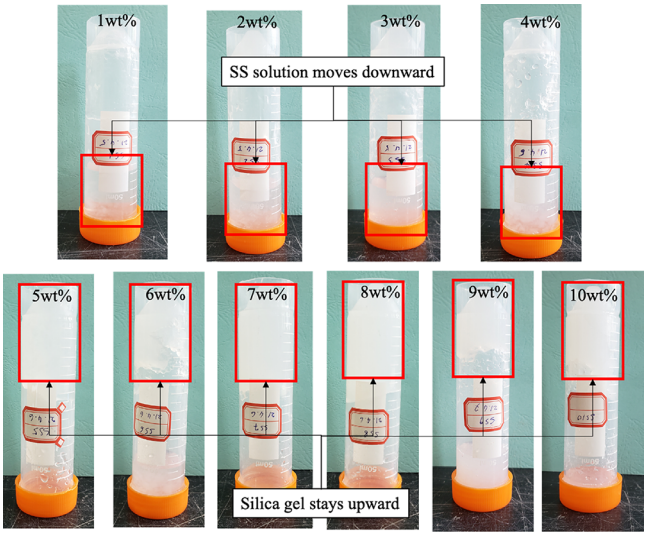

Figure 6. Formation of silica gel after a reaction between CO_2 and SS.

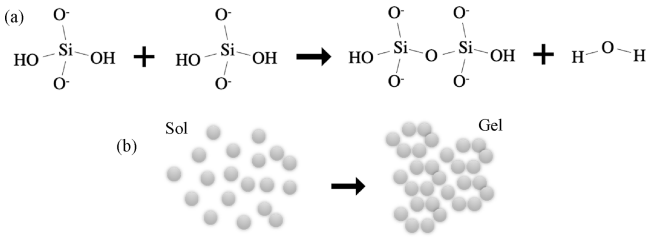

Figure 7. Silica gel formation once pH reduces: (a) polymeric silica forms by the Si−O−Si bond and (b) silica sol aggregates to become gels.

When the SS content was above the gelling concentration (5 to 10 wt %), the phase change from SS solution to silica gel is a rapid process when CO_2 dissolution within the solution becomes saturated.[36] This was reflected by the observation in the pH change in Figure 9a. The same observation was found in the literature.[37,38] HCl and H_2SO_4 were used to lower the pH of the sodium silicate solution, and silica gel was found to form in the pH range between 6 and 8. In our study, we further inspected that the gelling pH could be higher with increasing concentration of sodium silicate. For instance, when the concentration rose above 8 wt %, the gelling pH was approximately 9 and higher. In this regard, the pH of the gel should be better presented by the pH difference (Figure 9b). In this sense, the required pH difference was 2.8 to turn the 5 wt %

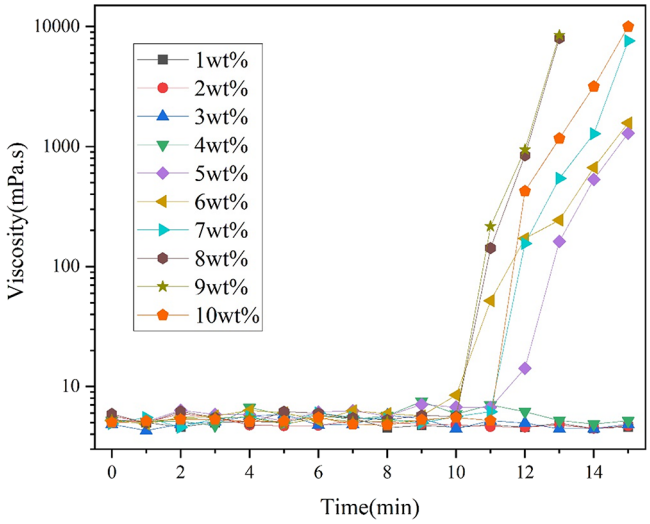

Figure 8. Effect of SS concentration on gel time.

SS solution into silica gel. The pH difference gradually decreased as the SS concentration increased, where only a 1.4 pH was needed in 10 wt %. Therefore, CO_2 neutralization is faster at higher SS concentrations. The main reason was that the amount of silica sol formed per unit of reduction in pH in a higher-SS concentration sample was greater, so the agglomeration of sol to develop gels was faster; thus, a lower pH difference was required and vice versa.

3.2. Effect of Ions on Silica Gel. The effect of ions and AW on the viscosity of the silica gel was investigated. The results are shown in Figure 10.

As shown, the efficiency of gelling by the reaction between SS and CO_2 was reduced by including various ions. The viscosity of the silica gel after the reaction gradually decreased from 8960 to 6266 mPa s, from 9487 to 5933 mPa s, from 9267 to 1000 mPa s, and from 8593 to 5070 mPa s for the concentration of Na^+ from 200 to 1000 ppm, the concentration of Ca^{2+} from 50 to 1000 ppm, the concentration of Mg^{2+} from 50 to 1000 ppm, and the concentration of SO_4^{2-} from 50 to 1000 ppm, respectively. On the other hand, the impact of HCO_3^- on gelling was less pronounced. The viscosity increased from 9240 to 9463 mPa s when including the HCO_3^- concentration from 200 to 2000 ppm, respectively. In the case of AW, the viscosity reduced from 10,000 to 8540 mPa s compared to DW.

As greater Na^+ ions were included in the deionized water prior to formulation of the SS solution, Na^+ then reacted with SS first and developed the precipitate. The solubility of SS was then

https://doi.org/10.1021/acsomega.2c00019
ACS Omega 2022, 7, 27090−27101

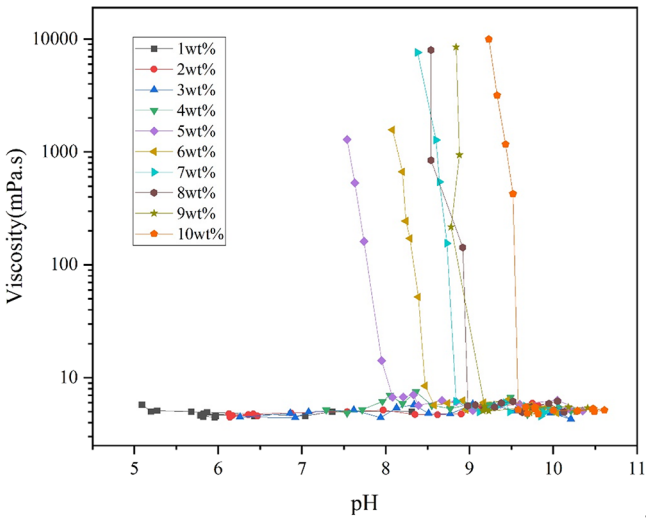

(a) pH monitoring during reaction

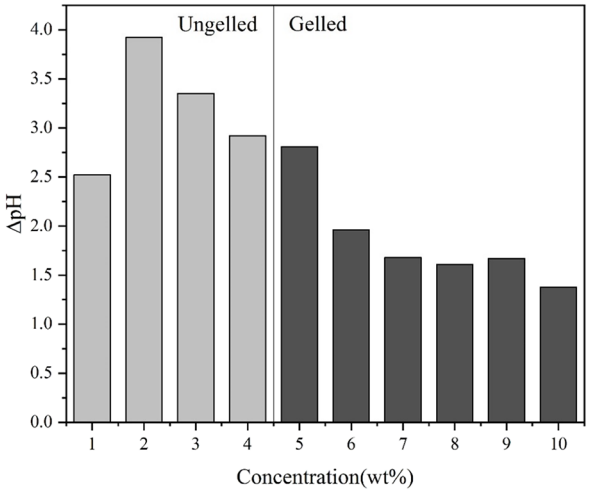

(b) Necessary pH reduction for silica gel development

Figure 9. (a,b) pH changes during the reaction.

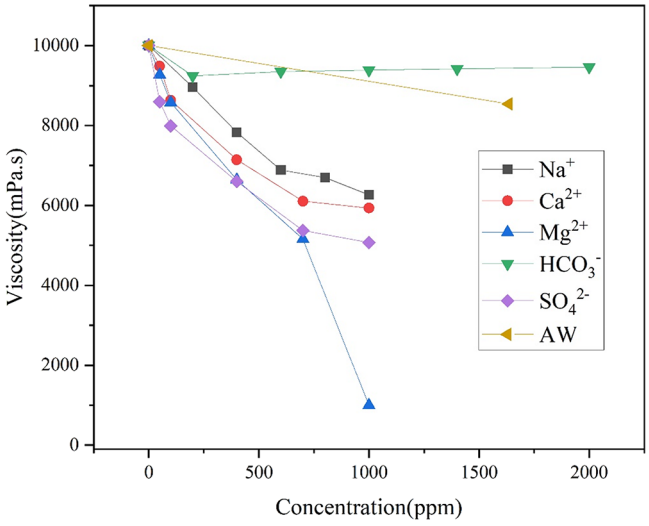

Figure 10. Effect of ions on the viscosity of the silica gel.

decreased at a higher Na^+ content due to the salting-out effect. Hence, lower silicate was available in the solution. Therefore,

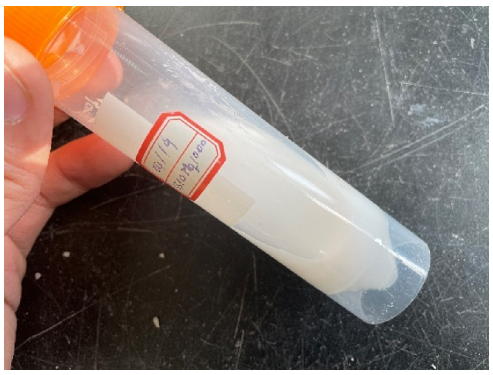

Figure 11. Ungelled SS solution with 1000 ppm Mg^{2+}.

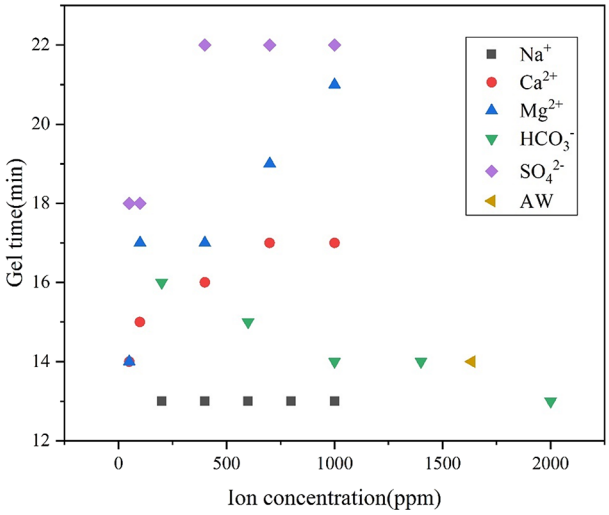

Figure 12. Effect of ions on gel time.

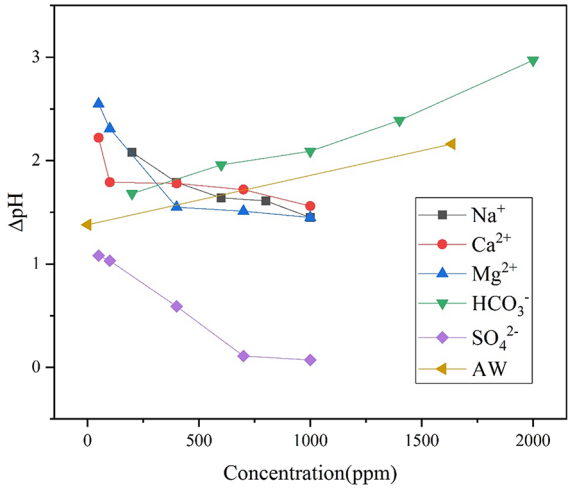

Figure 13. Effect of ions on pH changes.

there was less silica gel formation after reacting with CO_2, resulting in a lower apparent viscosity. This was also reported in the literature.[39]

There was a debate about the inclusion of divalent ions of Ca^{2+} and Mg^{2+} within SS solution on gelling purposes. Hamouda and Amiri[40] addressed that divalent ions accelerated SS gelling, and the product was found to have a higher strength. This was in contrast to what we found during the test; the SS solution

https://doi.org/10.1021/acsomega.2c00019
ACS Omega 2022, 7, 27090−27101

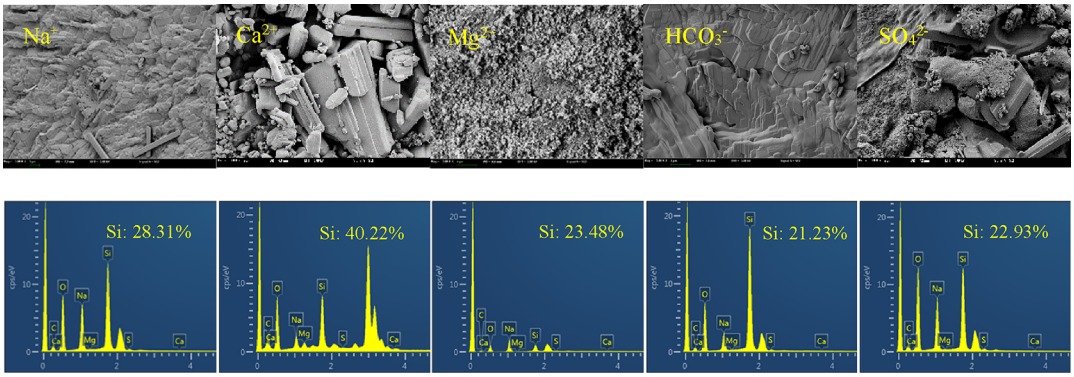

Figure 14. SEM images and elemental analysis of silica gel formulated with ions.

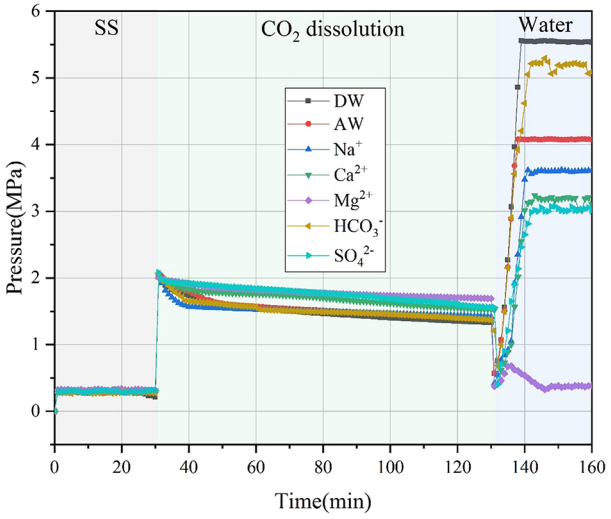

Figure 15. Grouting test.

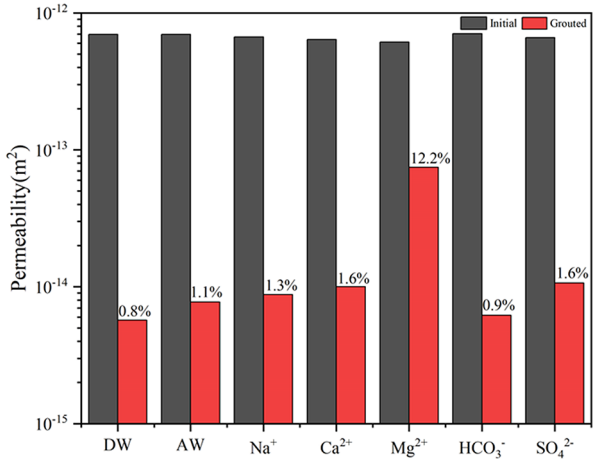

Figure 16. Permeability of the rock sample before and after grouting.

became cloudy with increasing concentrations of Ca^{2+} and Mg^{2+}, as shown in Figure 11. The cloudiness was plausibly due to metal silicate precipitates that are less soluble.[41] The effect of Ca^{2+} and Mg^{2+} on silica gel polymerization by CO_2 dissolution is similar. As presented in eqs 7 and 8, the added $CaCl_2$ and $MgCl_2$ react with SS to produce calcium silicate hydrate (C−S−H) and magnesium silicate hydrate (M−S−H), respectively. As a result, the formation of silica gels by the CO_2 reaction decreases with increasing Ca^{2+} and Mg^{2+}. Moreover, it is plausible that due to the lower molecular weight of Mg^{2+}, more $MgCl_2$ than $CaCl_2$ was required to formulate the same concentration of Ca^{2+} and Mg^{2+} ionic water. More silicate is then consumed from the solution to produce a hydrate or a precipitate rather than silica gel, which resulted in a lower apparent viscosity. It should be noted that no silica gel was developed after the CO_2 reaction at 1000 ppm Mg^{2+}. This implies that silicate is not available in the system when the cation concentration increases above its saturation point.

$$Na_2SiO_3 + CaCl_2 + xH_2O \rightarrow CaSiO_3{\cdot}xH_2O(C-S-H) + 2NaCl \quad (7)$$

$$Na_2SiO_3 + MgCl_2 + xH_2O \rightarrow MgSiO_3{\cdot}xH_2O(M-S-H) + 2NaCl \quad (8)$$

In the case of anions, Na_2SO_4 is dissolved in deionized water to produce Na^+ and SO_4^{2-}, and the solution is neutral. Although their reaction to SS is minimal, the solution thickened at a higher concentration. As a result, the dissolution of CO_2 becomes lower, which restricts the formation of silica gel. On the other hand, $NaHCO_3$ dissolves in deionized water to produce Na^+ and HCO_3^-. HCO_3^- further breaks into CO_3^{2-} and H^+. As addressed by Ren et al.,[42] when contacting with SS, the gelling occurs via the absorption of the H^+ in $NaHCO_3$ solution by SS, thus producing SiO_2 and Na_2CO_3 (eq 9). Therefore, HCO_3^- works as the cogelling agent during the CO_2 reaction.

$$Na_2SiO_3 + NaHCO_3 \rightarrow nSiO_2 + H_2O + Na_2CO_3 \quad (9)$$

To verify this, the effect of ions on gel time was monitored. The results are given in Figure 12.

As a result, HCO_3^- was found to accelerate the reaction rate, and the gel time was reduced from 16 to 13 min thanks to H^+ released by dissolving $NaHCO_3$ within the solution. The Na^+ ion constantly reduced the reaction time to 13 min regardless of its concentration. Ca^{2+}, Mg^{2+}, and SO_4^{2-} agreed well with their corresponding apparent viscosity. The gel time increased from 15 to 17 min, 14 to 21 min, and 18 to 22 min for Ca^{2+}, Mg^{2+}, and SO_4^{2-}, respectively. For AW in this case, the gel time was 14 min. The results agreed with the literature,[40,43] where a shorter gelation time was observed in a low concentration of dissolved salts.

The effect of ions on the change in pH during gelation was investigated. The results are given in Figure 13.

The pH changes in the gelling process are in a relationship with apparent viscosity. For instance, pH changes of Na^+, Ca^{2+}, Mg^{2+}, and SO_4^{2-} were reduced in the concentrated ion. This

https://doi.org/10.1021/acsomega.2c00019
ACS Omega 2022, 7, 27090−27101

Table 5. Properties of the Rock Sample

no.	D (10^{-2} m)	L (10^{-2} m)	V (m^3)	ϕ (%)	k_i (10^{-15} m^2)	k_g (10^{-15} m^2)
DW	2.53	100.21	503.53	12.3	697.35	5.70
AW	2.55	100.20	511.47	12.3	697.59	7.74
Na^+	2.52	100.25	499.75	12.1	668.72	8.77
Ca^{2+}	2.51	100.23	495.70	11.9	639.23	10.00
Mg^{2+}	2.55	100.20	511.47	11.6	613.66	74.76
HCO_3^-	2.53	100.24	503.68	12.5	705.49	6.19
SO_4^{2-}	2.54	100.22	507.56	12.0	659.23	10.65

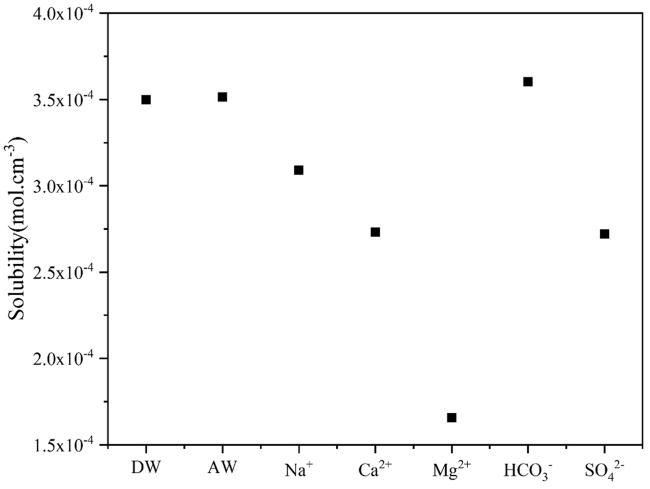

Figure 17. Effect of ions on CO_2 solubility within the SS solution.

agreed well with the reduction in apparent viscosity, where the formation of silica gel was disturbed by various mechanisms given in the above section. In this sense, the availability of silica in the solution was reduced, which then required a smaller amount of CO_2 to induce silica gel agglomeration. In contrast, the initial pH was higher as a result of the formation of NaOH from the higher HCO_3^- concentration. Therefore, the pH change required to develop a silica gel increased with concentration. The pH changes by AW also increased in comparison to DW as a reference case.

To further validate the discussion provided, we investigated the gel formulated under the effect of various ions for its morphology and elemental composition under SEM-EDS analysis. The results are presented in Figure 14. The gel structure was more consistent when Na^+ and HCO_3^- were included, where the Si concentration was 28.31 and 40.22%, respectively. The results were well in agreement with the measured apparent viscosity, where more silicate was available in the solution, thus creating more silica gel after the CO_2 reaction. On the contrary, a loose gel structure was observed in Ca^{2+}, Mg^{2+}, and SO_4^{2-} with Si concentrations of 23.48, 21.23, and 22.93%, respectively. Various ions consumed silicate from SS solution with different extents. Therefore, the silica gel developed by the CO_2 reaction with the SS solution depends on the silicate available in the solution.

3.3. Grouting Test. The grouting test by a reaction between CO_2 and SS solution was studied considering dissolved ions and AW. The results are given in Figure 15.

Grouting could be divided into three main sequences. In the first sequence, SS was injected from 0 to 30 min; the pressure in this step was relatively more stable, indicating good injectivity,[44] where the pressure change was approximately 0.3 MPa on average. The initial viscosity of the SS could travel without obstruction within the pores and fractures of the rock. Only in the cases of presaturation with Ca^{2+} and Mg^{2+}, the pressure slightly increased at the later stage of SS injection (approximately at 28 to 30 min). This was caused by the precipitation of SS after the divalent ion interaction, as explained earlier and illustrated in Figure 11, which narrowed the flow path of the injecting fluid. CO_2 was injected in the second sequence; thus, the pressure increased rapidly to approximately 2 MPa. From this stage, one could observe that the pressure change followed two patterns. The pressure changed exponentially in the early stage followed by a steady drop until equilibrium at 130 min for the presaturation of DW, AW, Na^+, and HCO_3^-. Among them, Na^+ and HCO_3^- possessed the most significant pressure changes in the early stage. Ca^{2+}, Mg^{2+}, and SO_4^{2-} rather followed a linear pressure change until equilibrium. However, the pressure reduction in the Mg^{2+} case was the least, indicating low CO_2 dissolution. As a result, the reduction in hydraulic conductivity when presaturated with Mg^{2+} water was low, around 0.4 MPa. As expected, the DW case achieved hydraulic pressures of 5.5 and 4 MPa for AW. The presaturation with ionic water induced hydraulic pressures of 5.2, 3.6, 3.1, and 3.0 MPa for HCO_3^-, Na^+, Ca^{2+}, and SO_4^{2-}, respectively.

3.4. Permeability Test. The permeability of the rock was determined at its initial stage and after grouting with various kinds of presaturated water. The summary of the results is shown in Figure 16 and Table 5.

The results agreed with the grouting experiment, where up to approximately 99% of the permeability of the rock was reduced regardless of the presaturated fluids. However, it failed in the case of Mg^{2+}, even though the permeability reduction was 87.8%. As suggested by the gelling test, Mg^{2+} at 1000 ppm caused precipitation rather than developing the gel during CO_2 dissolution. Precipitates narrowed flowing paths within the rock but could not effectively stop the water flow. Therefore, the reduction in hydraulic conductivity was relatively weak. The same observation was found for other ions. For instance, up to 98.7% of permeability was reduced by presaturation of Na^+ water, but the hydraulic pressure was 3.6 MPa. On the other hand, the hydraulic pressure in the case of presaturation with AW was 4 MPa, while its permeability reduction was 98.9%.

3.5. Solubility. The amount of CO_2 trapped within the rock voids was determined and expressed in terms of solubility, as shown in Figure 17.

In an ideal case, the solubility of CO_2 in silica gel was 3.5×10^{-4} mol/cm^3. It was found that the effect of AW and HCO_3^- on CO_2 solubility was minimal, where the solubility was 3.51×10^{-4} and 3.6×10^{-4} mol/cm^3, respectively, indicating that the current approach is suitable for the target mining site. On the other hand, the CO_2 solubility was reduced by 11.6, 21.9, 52.6, and 22.2% for the presaturation of Na^+, Ca^{2+}, Mg^{2+}, and SO_4^{2-} ions.

Overall, the solubility of CO_2 within the SS solution was effective in both the ideal case (DW) and the average mining

https://doi.org/10.1021/acsomega.2c00019
ACS Omega 2022, 7, 27090−27101

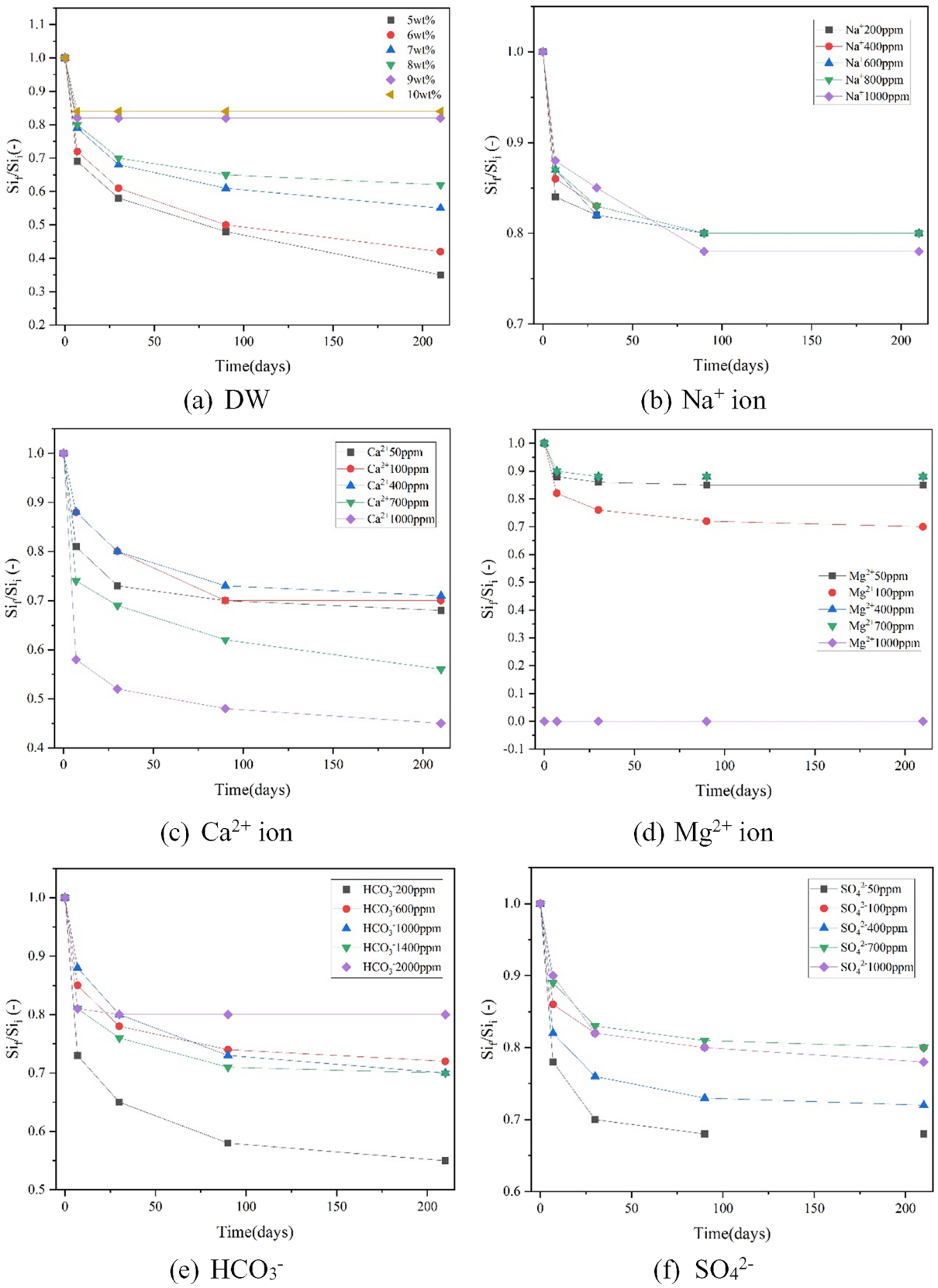

Figure 18. (a–f) Change in silica concentration against time.

environment (AW). However, the trapping capability of CO_2 using SS solution was lowered in the harsh environment where the concentration of certain ions was elevated.[45]

3.6. Degradation of Silica Gel. The available silica gel was investigated under ambient conditions. The results are given in Figures 18 and 19.

https://doi.org/10.1021/acsomega.2c00019
ACS Omega 2022, 7, 27090−27101

Figure 19. Degradation of silica gel.

Table 6. Summary of the Effect of SS and Ions on Grouting Parameters[a]

	viscosity	gel time	hydraulic conductivity reduction	CO_2 solubility	permeability reduction	stability
SS	ΔΔ	ΔΔ	Δ	Δ	Δ	ΔΔ
Na^+	ΔΔ	Δ	∇	∇	∇	-
Ca^{2+}	Δ∇	Δ∇	∇	∇	∇	Δ∇
Mg^{2+}	Δ∇	Δ∇	∇	∇	∇	-
HCO_3^-	-	ΔΔ	Δ	Δ	Δ	ΔΔ
SO_4^{2-}	Δ∇	Δ∇	∇	∇	∇	ΔΔ

[a]ΔΔ defines that the higher the concentration, the better; Δ∇ defines that the higher the concentration, the worse; Δ defines good; ∇ defines worse; - defines neutral.

The degradation of silica gel was dependent on the concentration of SS. At lower concentrations of SS, the silica gel (Si_i) was reversible to a liquid form starting from 7 days and continuing until 210 days. For example, only 35 and 42% silica gel (Si_f/Si_i) was observed at 210 days using SS concentrations of 5 and 6 wt %, respectively. On the contrary, more silica gel was observed at a higher SS concentration. The degradation was ended at day 7 using 10 wt % SS, where up to 84% of silica gel was still available. Regardless of the initial concentration of SS, the attachment of the silica gel to the surface of the tube was better when it was formulated without dissolved ions (Figure 19).

There was no significant effect on silica gel degradation when Na^+ and Mg^{2+} ions were included, where the degradation rate was similar to that of DW. On the other hand, the effect of the Ca^{2+} ion on the stability of the silica gel increased linearly with its concentration, where up to 55% of silica gel was reversible to a liquid phase after 210 days.

In the case of anions, more silica gel was observed at a higher concentration of HCO_3^- and SO_4^{2-}. Degradation decreased from 45 to 20% and from 78 to 68% for the HCO_3^- and SO_4^{2-} ions, respectively.

3.7. Summary and Limitations. On the basis of the above experimental results, the effect of SS concentration and ions on grouting parameters is summarized in Table 6.

https://doi.org/10.1021/acsomega.2c00019
ACS Omega 2022, 7, 27090−27101

The conclusion of the scanning criteria could be drawn on each parameter. To increase the viscosity or strength of the silica gel, the initial concentration of SS in the liquid phase should be higher, but the dissolved ions reduced the viscosity of the silica gel except HCO_3^-. The gel time was shortened by the increase of SS, Na^+, and HCO_3^- concentration. Hydraulic conductivity reduction and CO_2 solubility possessed the same pattern, where ions lowered the hydraulic conductivity reduction efficiency and CO_2 dissolution caused by the decrease in gel strength. The stability of the developed silica gel was found to be more stable at higher concentrations of SS, HCO_3^-, and SO_4^{2-}, while Ca^{2+} possessed a reverse effect. However, Na^+ and Mg^{2+} did not show a significant effect on the stability of the silica gel.

4. CONCLUSIONS

The present study resolved the grouting issue of microcracks, enabling hydraulic conductivity reduction, simultaneously enhancing CO_2 utilization in underground construction, achieving CO_2 capture while grouting (CCG). Systematic experiments considering the effects of dissolved ions of aquifer water were conducted. Based on the above results, the following conclusions could be drawn.

1. Stable and high-strength silica gel was formed by CO_2 reacting with SS with a concentration greater than 5 wt %. The developed silica gel could be described as a power law fluid with a pseudoplastic behavior.
2. Na^+, Ca^{2+}, Mg^{2+}, and SO_4^{2-} ions were found to decrease gel strength observed by a reduction in viscosity and precipitation. Nevertheless, the effect on gel strength was not pronounced by HCO_3^- and aquifer water.
3. The silica gel was capable to achieve a hydraulic pressure of up to 5.5 MPa. Presaturation of ionic and aquifer waters was found to lower the hydraulic pressure but still achieved the lowest pressure of 3 MPa. However, grouting is not suitable to use when the Mg^{2+} ion concentration is above 1000 ppm.
4. At a 2 MPa grouting pressure, CO_2 was found to solubilize up to 3.51×10^{-4} mol/cm^3 within the silica gel with a presaturation of aquifer water.
5. The silica gel was found to be more stable at higher concentrations of SS (9 and 10 wt %). The harsh concentrations of Na^+, HCO_3^-, and SO_4^{2-} did not affect the stability of the silica gel except Ca^{2+} and Mg^{2+}.

AUTHOR INFORMATION

Corresponding Authors

Ichhuy Ngo − *Key Laboratory of Deep Coal Resource Mining, China University of Mining & Technology, Ministry of Education, Xuzhou 221116, China;* orcid.org/0000-0002-6029-1239; Email: tbh230@cumt.edu.cn

Liqiang Ma − *Key Laboratory of Deep Coal Resource Mining, China University of Mining & Technology, Ministry of Education, Xuzhou 221116, China*; Email: ckma@cumt.edu.cn

Authors

Jiangtao Zhai − *Key Laboratory of Deep Coal Resource Mining, China University of Mining & Technology, Ministry of Education, Xuzhou 221116, China*

Yangyang Wang − *Key Laboratory of Deep Coal Resource Mining, China University of Mining & Technology, Ministry of Education, Xuzhou 221116, China*

Tianxiang Wei − *Key Laboratory of Deep Coal Resource Mining, China University of Mining & Technology, Ministry of Education, Xuzhou 221116, China*

Yanxiao Ni − *School of Foreign Studies, China University of Mining & Technology, Ministry of Education, Xuzhou 221116, China*

Complete contact information is available at: https://pubs.acs.org/10.1021/acsomega.2c00019

Notes

The authors declare no competing financial interest.

ACKNOWLEDGMENTS

The authors would like to express their appreciation to the National Natural Science Foundation of China (51874280) and the Fundamental Research Funds of the Central Universities (2021ZDPY0211) for financial support.

REFERENCES

(1) He, G.; Zhang, H.; Xu, Y.; Lu, X. China's clean power transition: Current status and future prospect. *Resour., Conserv. Recycl.* **2017**, *121*, 3−10.

(2) Long, R.; Li, H.; Wu, M.; Li, W. Dynamic evaluation of the green development level of China's coal-resource-based cities using the TOPSIS method. *Res. Policy* **2021**, *74*, No. 102415.

(3) Lin, B.; Bega, F. China's Belt & Road Initiative coal power cooperation: Transitioning toward low-carbon development. *Energy Policy* **2021**, *156*, No. 112438.

(4) Xu, K.; Dai, G.; Duan, Z.; Xue, X. Hydrogeochemical evolution of an Ordovician limestone aquifer influenced by coal mining: a case study in the Hancheng mining area, China. *Mine Water Environ.* **2018**, *37*, 238−248.

(5) Xu, Y.; Ma, L.; Khan, N. M. Prediction and Maintenance of Water Resources Carrying Capacity in Mining Area—A Case Study in the Yu-Shen Mining Area. *Sustainability* **2020**, *12*, 7782.

(6) Ma, L.; Guo, J.; Liu, W.; Zhang, D.; Yu, Y. Water conservation when mining multiple, thick, closely-spaced coal seams: A case study of mining under Weishan Lake. *Mine Water Environ.* **2019**, *38*, 643−657.

(7) Zhang, C.; Wang, F.; Bai, Q. Underground space utilization of coalmines in China: A review of underground water reservoir construction. *Tunnelling Underground Space Technol.* **2021**, *107*, No. 103657.

(8) Dong, S.; Xu, B.; Yin, S.; Han, Y.; Zhang, X.; Dai, Z. Water Resources Utilization and Protection in the Coal Mining Area of Northern China. *Sci. Rep.* **2019**, *9*, 1214.

(9) Sui, W.; Liu, J.; Hu, W.; Qi, J.; Zhan, K. Experimental investigation on sealing efficiency of chemical grouting in rock fracture with flowing water. *Tunnelling Underground Space Technol.* **2015**, *50*, 239−249.

(10) Liang, Y.; Sui, W.; Qi, J. Experimental investigation on chemical grouting of inclined fracture to control sand and water flow. *Tunnelling Underground Space Technol.* **2019**, *83*, 82−90.

(11) Ngo, I.; Ma, L. Q.; Zhai, J. T.; Wang, Y. Y. *Feasibility of CO2 as a curing agent for silicate-based grouting gel in fractures after coal mining*; 2021 2021, 2021, European Association of Geoscientists & Engineers, 1 ed., pp. 1−5.

(12) Zhang, H. B.; et al. Research and application of micro-nano inorganic grouting materials. *J. China Coal. Soc.* **2020**, *45*, 949−955.

(13) Guo, H.; Li, B.; Zhang, Y.; Wang, X.; Zhang, F. Hydrophilic characteristics of soft rock in deep mines. *Int. J. Min. Sci. Technol.* **2015**, *25*, 177−183.

(14) Zheng, P. Q.; Chen, W. Z.; Tan, X. J.; Dai, Y. H. Study of failure mechanism of floor heave and supporting technology in soft rock of large deformation roadway. *Chin. J. Rock Mech. Eng.* **2015**, *34*, 3143−3150.

(15) M.-S., Wang, M., Huangfu, Key problems on subsea tunnel construction. *Journal of Architectural Science and Engineering* vol. *4*, **2005**.

(16) R. W., Henn, N. C., Soule, *Ultrafine cement in pressure grouting*; American Society of Civil Engineers, 2010.
(17) Eklund, D.; Stille, H. Penetrability due to filtration tendency of cement-based grouts. *Tunnelling Underground Space Technol.* **2008**, *23*, 389−398.
(18) Butrón, C.; Gustafson, G.; Fransson, Å.; Funehag, J. Drip sealing of tunnels in hard rock: A new concept for the design and evaluation of permeation grouting. *Tunnelling Underground Space Technol.* **2010**, *25*, 114−121.
(19) Zhou, X.; Ding, W.; He, J.; Li, A.; Sun, Y.; Wang, X. Microfractures in the middle Carboniferous carbonate rocks and their control on reservoir quality in the Zanaral Oilfield. *Mar. Pet. Geol.* **2018**, *92*, 462−476.
(20) Apaydin, O. G.; Ozkan, E.; Raghavan, R. Effect of discontinuous microfractures on ultratight matrix permeability of a dual-porosity medium. *SPE Reservoir Eval. Eng. Conf. Pap.* **2012**, *15*, 473−485.
(21) Zhang, W. et al. Fissure Grouting Mechanism Accounting for the Time-Dependent Viscosity of Silica Sol. *ACS Omega* , *6* (), 28140−28149, 2021/10/26 2021.
(22) Ngo, I.; Sasaki, K.; Ma, L.; Nguele, R.; Sugai, Y. Enhancing surfactant desorption through low salinity water post-flush during Enhanced Oil Recovery. *Oil Gas Sci. Technol.* **2021**, *76*, 68.
(23) Speight, J. G. 3 - Water chemistry In *Natural Water Remediation*; Butterworth-Heinemann, 2020, pp. 91−129.
(24) Zullo, R.; et al. Effect of rheology evolution of a sustainable chemical grout, sodium-silicate based, for low pressure grouting in sensitive areas: Urbanized or historical sites. *Constr. Build. Mater.* **2020**, *230*, No. 117055.
(25) Li, S.; et al. Adaptability of polyurethane/water glass grouting reinforcement to subsea tunnels. *Constr. Build. Mater.* **2021**, *311*, No. 125354.
(26) Lu, G.; Wang, Y.-S.; Zhang, Y.; Ariaratnam, S. T. Feasibility of using sodium silicate as grouting in loose coal bed sections for methane drainage. *Tunnelling Underground Space Technol.* **2018**, *72*, 107−113.
(27) Hatzignatiou, D. G.; Askarinezhad, R.; Giske, N. H.; Stavland, A. Laboratory testing of environmentally friendly sodium silicate systems for water management through conformance control. *SPE Prod. Oper.* **2016**, *31*, 337−350.
(28) Lakatos, I.; Lakatos-Szabo, G.; Szentes, G. Revival of Green Conformance and IOR/EOR Technologies: Nanosilica Aided Silicate Systems - A Review In *SPE International Conference and Exhibition on Formation Damage Control*; Society of Petroleum Engineers, 2018.
(29) Liu, S.; Ott, W. K. Sodium silicate applications in oil, gas & geothermal well operations. *J. Pet. Sci. Eng.* **2020**, *195*, No. 107693.
(30) Birol, F. *An energy sector roadmap to carbon neutrality in China* IEA: Paris, 2021.
(31) Yahia, A.; Mantellato, S.; Flatt, R. J. 7 - Concrete rheology: A basis for understanding chemical admixtures. In *Science and Technology of Concrete Admixtures*; Aïtcin, P.-C.; Flatt, R. J. Eds.: Woodhead Publishing, 2016, pp. 97−127.
(32) McDonald, M., Ott Miller, N. W.; Elphingstone, G. Silica gel as an economical and innovative alternative to bio-based polymers in aqueous hydraulic fracturing fluids 2016, AADE Houston: Texas.
(33) Padmanabhan, M.; Bhattacharya, M. Flow behavior and exit pressures of corn meal under high-shear−high-temperature extrusion conditions using a slit diea. *J. Rheol.* **1991**, *35*, 315−343.
(34) Fraiha, M.; Biagi, J. D.; Ferraz, A. C. d. O. Rheological behavior of corn and soy mix as feed ingredients. *Food Sci. Technol.* **2011**, *31*, 129−134.
(35) Loodts, V.; Rongy, L.; De Wit, A. Impact of pressure, salt concentration, and temperature on the convective dissolution of carbon dioxide in aqueous solutions. *Chaos* **2014**, *24*, 043120.
(36) Fleury, M.; Sissmann, O.; Brosse, E.; Chardin, M. A silicate based process for plugging the near well bore formation. *Energy Procedia* **2017**, *114*, 4172−4187.
(37) Supiyani; Agusnar, H.; Sugita, P.; Nainggolan, I. Preparation sodium silicate from rice husk to synthesize silica nanoparticles by sol-gel method for adsorption water in analysis of methamphetamine. *S. Afr. J. Chem. Eng.* **2022**, *40*, 80−86.
(38) Katoueizadeh, E.; Rasouli, M.; Zebarjad, S. M. A comprehensive study on the gelation process of silica gels from sodium silicate. *J. Mater. Res. Technol.* **2020**, *9*, 10157−10165.
(39) Engelhardt, H.-J.; von Borstel, L. E. The behaviour of sodium silicate solutions (water glass) in the saline environment and their use in salt mining. *Z. Dtsch. Ges. Grundwasser* **2014**, *165*, 115−122.
(40) Hamouda, A. A.; Amiri, H. A. A. Factors affecting alkaline sodium silicate gelation for in-depth reservoir profile modification. *Energies* **2014**, *7*, 568−590.
(41) Bauer, S.; Gronewald, P.; Hamilton, J.; LaPlant, D.; Mansure, A.. *High-temperature plug formation with silicates*; OnePetro, 2005.
(42) Ren, X.; Hu, X.; Xue, D.; Li, Y.; Shao, Z.; Dong, H.; Cheng, W.; Zhao, Y.; Xin, L.; Lu, W. Novel sodium silicate/polymer composite gels for the prevention of spontaneous combustion of coal. *J. Hazard. Mater.* **2019**, *371*, 643−654.
(43) Pham, L. T.; Hatzignatiou, D. G. Rheological evaluation of a sodium silicate gel system for water management in mature, naturally-fractured oilfields. *J. Pet. Sci. Eng.* **2016**, *138*, 218−233.
(44) Ngo, I.; Sasaki, K.; Nguele, R.; Sugai, Y. Formation damage induced by water-based alumina nanofluids during enhanced oil recovery: influence of postflush salinity. *ACS Omega* **2020**, *5*, 27103−27112.
(45) E., Perkins, A., Innovates, *Fundamental geochemical processes between CO2, water and minerals*; Alberta Innovates−Technology Futures, 2003.

https://doi.org/10.1021/acsomega.2c00019
ACS Omega 2022, 7, 27090−27101